ISIJ International, Vol. 42 (2002), No. 12, pp. 1326–1333

*Review*

# Scanning Electrochemical Microscopic Study of Detecting Non-homogeneity in Surface Reactions of Metals

K. FUSHIMI and M. SEO

Graduate School of Engineering, Hokkaido University, Kita-13 Jo, Nishi-8 Chome, Kita-ku, Sapporo 060-8628 Japan.

(*Received on May 24, 2002; accepted in final form on August 26, 2002*)

Scanning electrochemical microscopy (SECM) is powerful to investigate non-homogeneity of surface reaction in solution. It is useful for evaluating the distribution of electrochemical reactions taking place on the electrode surface such as corrosion reaction, redox reaction on passive film and so on. The heterogeneous electrochemical reaction on polycrystalline iron, titanium and single crystal magnetite electrode surfaces were discussed. SECM can be also employed for inducing locally a certain surface electrochemical reaction on the specimen by operating a probe electrode as liquid-phase ion gun (LPIG). The application of LPIG to the passive film formed on iron for inducing the local film breakdown has revealed the details of its local breakdown process.

KEY WORDS: scanning electrochemical microscopy; non-homogeneity; surface reaction; passive film; local breakdown; pitting corrosion; iron; titanium; single crystal magnetite.

## 1. Introduction

Surface reaction is in general classified into non-homogeneous one because it takes place at the interface between two phases at least. Corrosion reaction of metals proceeds at the interface between metal and solution when dissolution of metals at anodic sites is coupled with cathodic reaction such as oxygen reduction or hydrogen evolution. Charge transfer in vertical direction to the surface: diffusion of chemical species from/to the interface or electron transfer reaction at the interface; determines the dissolution rate. Since the reactions are not localized, that is, homogeneous in horizontal direction to the surface, the dissolution rate can be represented by current density which is defined with dissolution current per unit of surface area.

On the other hand, some surface reactions proceeds locally. In these cases, non-homogeneity in horizontal direction to the surface is important as well as one in vertical direction because fluctuation in surface properties would give differences in dynamics and kinetics of the surface reaction. For example, pitting corrosion takes place at the site where the passive film on metal is locally broken down in solution containing aggressive ions. The induction of the local breakdown changes the passive metal surface from stable homogeneous state to localized heterogeneous state and finally a pit is formed. In pitting corrosion, real dissolution rate should be calculated from dissolution current per size of each pit. This means that dissolution current and size for every pit have to be measured even if a number of pits form and/or diminish.

From the above view-points, it is necessary to investigate non-homogeneous surface reaction in horizontal direction as well as in vertical. Recently various experimental methods of detecting non-homogeneous surface reaction have been developed and applied to fields of surface science. Scanning electrochemical microscopy (SECM)[1,2] is one of powerful tools for investigating non-homogeneous reaction at interface in solutions. The SECM probe consisting of a micro-disk electrode can detect Faradaic current near the interface. Therefore scanning probe electrode allows to address the electroactive sites and to image the distribution of electrochemical activity at the interface. Furthermore the probe electrode can be used as a local generator to induce new species electrochemically to the interface. In this paper, the results of SECM applied to corrosion field will be reviewed and discussed.

## 2. SECM

For detecting non-homogeneous in surface reactions, information of surface geometrical parameters is collected by scanning a "probe" above the surface. In case of SECM, the probe is a micro-disk electrode with the following features and benefits[3]:

(1) fast attainment to a steady-state current or semi steady-state current
(2) less contribution for charging current
(3) high sensitivity and rapid response to measurement
(4) ability of measuring chemical or electrochemical reaction rates under the steady-state
(5) usability in solvents with low polarity or in solvents containing a small amount of electrolyte
(6) capability of measuring electrochemical reactions of electrolyte itself
(7) facility of monitoring local events of electroactive species

(8) induction of electrochemical interaction by combination of microelectrodes

The SECM probe electrode acts as a working electrode as well as a specimen electrode in an electrochemical cell as shown in **Fig. 1**. Both working electrodes are connected with a bipotentiostat to control potentials, independently, and to flow current against a counter electrode. SECM probe electrode works electrochemically and flows Faradaic current above the specimen electrode surface.

In case of electrochemical reaction on a micro-disk electrode under diffusion-controlled conditions, a hemispherical diffusion layer of reactant species forms on the microelectrode. The diffusion limiting current, $I_{limit}$, flowing through the microelectrode, which is located in solution bulk, is expressed as follows.[4)]

$$I_{limit}=4nDFc^{*}a \quad \text{.....(1)}$$

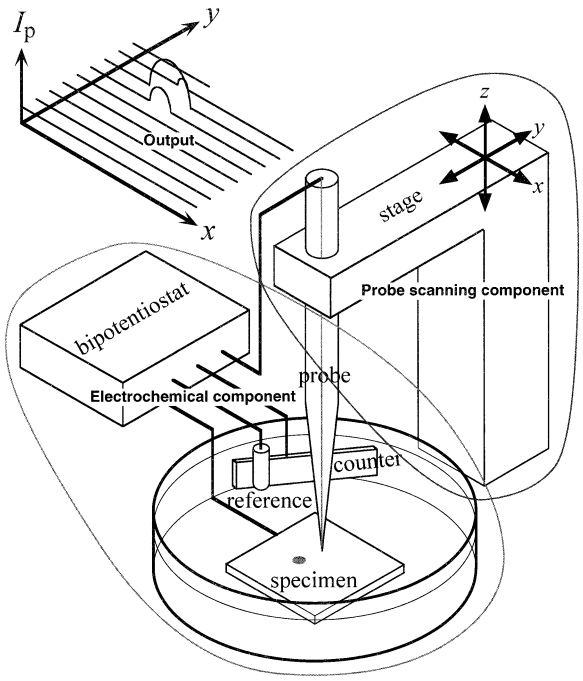


**Fig. 1.** Schematic diagram of SECM apparatus.

where $n$ is the number of electrons passed per reacted atom, $F$ is the Faraday constant, $a$ is the radius of employed disk electrode, $D$ and $c^{*}$ are the diffusion coefficient and bulk concentration of reactant species, respectively. On the other hand, when the micro-disk electrode approaches the specimen surface as a probe electrode of SECM, the limiting current flowing through the microelectrode changes depending on the distance between the probe and specimen electrodes, and on the electrochemical activity of the specimen surface as well as the mode adapted in SECM. This is due to the deformation of diffusion layer on the microelectrode as shown in **Fig. 2**. If the specimen is an insulator, the probe current decreases with decreasing distance above the specimen surface because no reactant species for the probe electrode are produced on the insulator surface. On the other hand, if the specimen is a good conductor, the probe current increases with decreasing distance above the specimen surface because the reactant species for the probe electrode are easily produced on the conductor surface and the positive feedback effect of redox reaction is operative between the microelectrode and specimen electrode.

Depending on potentials of both working electrodes and shapes of diffusion layer on electrodes, SECM is classified into three modes, *i.e.*, feedback (FB), tip generation/substrate collection (TG/SC), and substrate generation/tip collection (TG/SC) modes. In FB mode, the specimen electrode is kept at an open circuit potential. The probe electrode can sense the conductivity of specimen surface by using feedback current flowed through the probe electrode. In both generation/collection modes, a couple of working electrodes are polarized. A collector electrode detects the products diffusing from a generator electrode. When the probe electrode is a generator, the field interacting between both electrodes is limited to the size of the probe electrode and the lateral resolution of SECM image is the same as one in FB mode. On the other hand, when the specimen electrode is a generator, the lateral resolution of SECM image is poor because the interacting field exceeds the size of the probe electrode can pick up. The details of the principle and theory have been discussed by Bard *et al.*[2,5–7)]

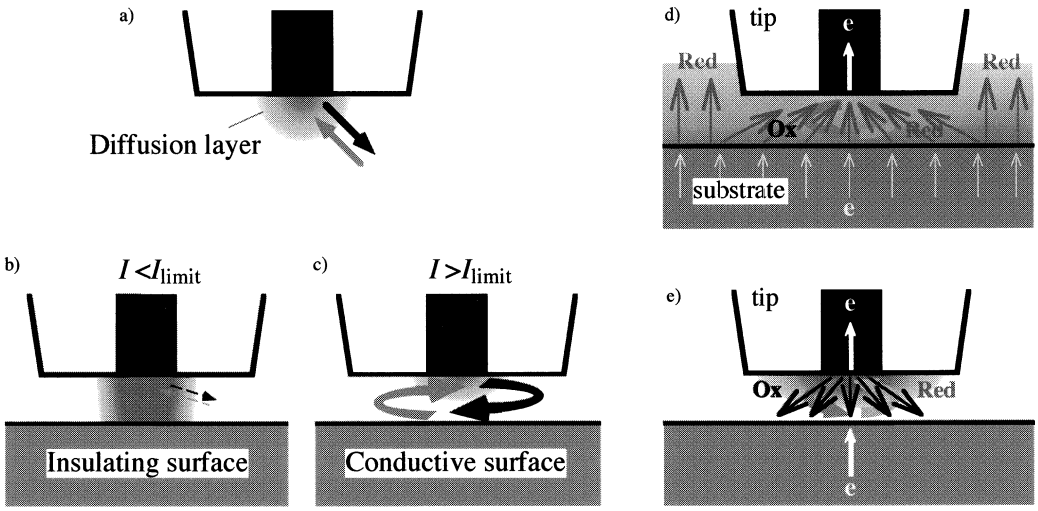


**Fig. 2.** Schematic diagram of the diffusion layer at the tip of probe electrode located a) at bulk solution or close to the surface of b) insulating or c) conductive specimen electrode in FB mode, d) SG/TC mode and e) TG/SC mode.

**Table 1.** SECM evaluation for heterogeneity of passive film.

| substrate | mediator | electrolyte | ref. |
|---|---|---|---|
| Cr | $MV^+/MV^{2+}$ * | $KCl + MVCl_2$ | 8 |
| | $Ru(NH_3)_6^{2+}/ Ru(NH_3)_6^{3+}$ | $K_2SO_4 + Ru(NH_3)_6Cl_3$ | 8 |
| | $Fe(CN)_6^{4-}/Fe(CN)_6^{3-}$ | $KCl + K_4Fe(CN)_6$ | 8 |
| Ti | $Ru(NH_3)_6^{2+}/ Ru(NH_3)_6^{3+}$ | $KCl + Ru(NH_3)_6Cl_3$ | 9 |
| | $Br^-/Br_2$ | $H_2SO_4/K_2SO_4 + KBr$ | 10-13 |
| | $Fe(CN)_6^{4-}/Fe(CN)_6^{3-}$ | $K_2SO_4$/NaCl/Borate + $K_4Fe(CN)_6$ | 12-15 |
| | $OH^-/O_2$ | $H_2SO_4$ | 15 |
| Ta | $I^-/I_3^-$ | $K_2SO_4 + KI$ | 16, 17 |
| | $Ru(NH_3)_6^{2+}/ Ru(NH_3)_6^{3+}$ | $K_2SO_4 + Ru(NH_3)_6Cl_3$ | 16 |
| | $Fe(CN)_6^{4-}/Fe(CN)_6^{3-}$ | $K_2SO_4 + K_4Fe(CN)_6$ | 16 |
| Fe | $Fe(CN)_6^{4-}/Fe(CN)_6^{3-}$ | Borate + $K_4Fe(CN)_6$ | 18, 19 |

*MV: methyl viologen

## 3. Non-homogeneity of Passive Films

Pitting corrosion starts when passive film is locally broken down and the repair is not sufficient. For better understanding of pitting corrosion, it is important to reveal non-homogeneity of passive film since the local breakdown would initiate preferentially at the thinnest or the most defective parts of the passive film. Several researchers have applied SECM to investigate non-homogeneity of passive film in solutions containing redox species as listed in **Table 1**. In all cases, the observed results depend strongly on the combination of redox species and SECM mode adapted.

### 3.1. Non-homogeneity of Passive Film Formed on a Polycrystalline Iron Electrode

Fushimi *et al.* have investigated the non-homogeneity of passive film formed on a polycrystalline iron electrode in pH 8.4 borate solution containing 0.03 mol dm$^{-3}$ $K_4Fe(CN)_6$ by using TG/SC mode of SECM in which a probe electrode was polarized at 1.2 V (SHE) to oxidize $Fe(CN)_6^{4-}$ while the passivated iron electrodes were polarized at 0.1 V (SHE) to reduce $Fe(CN)_6^{3-}$ on passive film surfaces.[18,19] The oxidation current of $Fe(CN)_6^{4-}$ flowed through the probe electrode depended on the distance between the probe and iron electrodes and the thickness of passive film as shown in **Fig. 3**. The relatively large probe current flowed above the thinner film surface as compared with the thicker one because the reduction of $Fe(CN)_6^{3-}$ on passive film surface is influenced by thickness and semiconductive properties of the film. The probe current image obtained by scanning probe electrode with a constant distance, therefore, gave the thickness distribution of passive film on a polycrystalline iron electrode as shown in **Fig. 4**. Furthermore it was found that the thicker film was formed on the grain oriented to {100} as compared with the grains oriented to {110} and {111}. This means that growth rate of the film depends on the substrate grain orientation even if the iron electrode is polarized at the same potential for formation of passive film.

### 3.2. Non-homogeneity of Passive Film Formed on a Polycrystalline Titanium Electrode

The passive film on titanium is the most frequently investigated material by using SECM because the relatively thicker film has sufficient stabilities for SECM measurements. In solutions containing bromide ions, however, the passive film on titanium is likely broken down. Smyrl *et al.* have imaged the active site of passive film above which the reduction of bromide ions takes place more easily on the probe electrode by using SG/TC mode of SECM.[10,11,21,22] Basame *et al.* also have imaged the oxidized surface of titanium or tantalum electrode where several numbers of sites become active and then less active asynchronously.[12,13,16,17] It was assumed that these active sites of passive film were attacked by bromide ions and broken down locally. The local breakdown may proceed at the sites of the thinner or more defective film under which the substrate titanium has sufficient defects or inclusions.

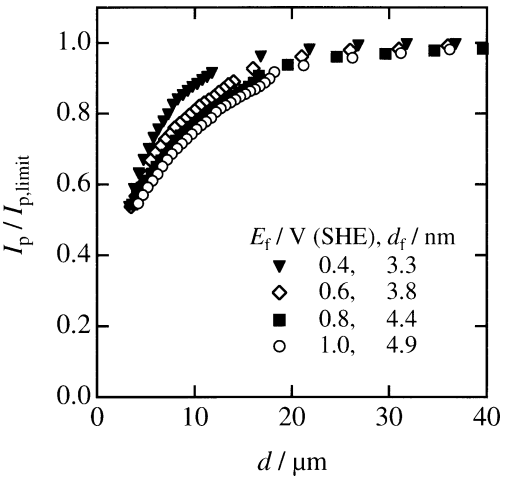


**Fig. 3.** Normalized probe current, $I_p/I_{p,limit}$, as a function of distance between probe and iron electrodes, $d$. The probe and iron electrodes were polarized at 1.2 and 0.1 V (SHE), respectively, in deaerated pH 8.4 borate solution containing 0.03 mol dm$^{-3}$ $K_4Fe(CN)_6$ after the iron electrode was passivated at $E_f$=0.4, 0.6, 0.8 or 1.0 V (SHE) for 3.6 ks in deaerated pH 8.4 borate solution. Thickness of passive film, $d_f$, was obtained from Azumi *et al.*[20]

On the other hand, Fushimi *et al.* have applied the TG/SC mode of SECM to investigate the non-homogeneity of passive film formed on a polycrystalline titanium electrode.[14] The larger probe current flowed more on the grain covered with the thinner film similar to the film formed on a polycrystalline iron. Fluctuation in probe current reflecting non-homogeneity of passive film is enhanced with increasing film formation potential as shown in **Fig. 5**. It was assumed from the combination with micro Raman spectroscopy that, at potentials more than 4 V (SHE), structural change of the film from amorphous to anatase takes place and induces the increase in the fluctuation. Furthermore Fushimi *et al.* have applied the SG/TC mode of SECM to image the distribution of oxygen evolution during anodic oxidation of a polycrystalline titanium electrode in $H_2SO_4$.[15] The probe electrode was employed to detect oxygen evolved from the tita-

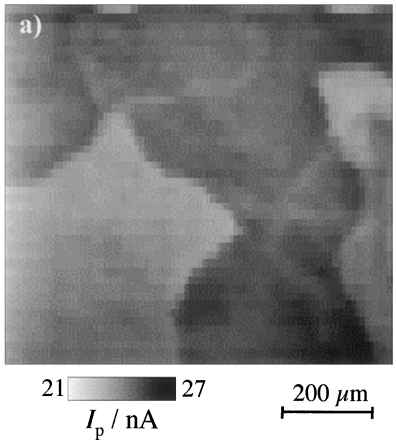


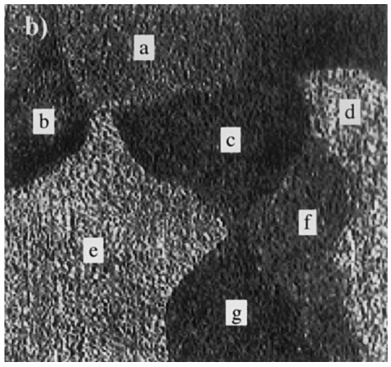


| | Index plane | rotation angle [100] | rotation angle [010] |
|---|---|---|---|
| a | $(\bar{0}11)$ | -10° | 5° |
| b | (111) | 0° | -5° |
| c | (101) | -5° | 15° |
| d | $(00\bar{1})$ | 10° | 0° |
| e | $(0\bar{0}1)$ | 10° | 0° |
| f | (101) | -10° | 5° |
| g | (101) | 0° | 15° |

**Fig. 4.** (a) Probe current image measured after the iron electrode surface with distinctive crystal grains was passivated at 1.0 V (SHE) for 3.6 ks. For measurement of the probe current image, the probe and iron electrodes were polarized at 1.2 and 0.1 V (SHE), respectively, in deaerated pH 8.4 borate solution containing 0.03 mol dm$^{-3}$ $K_4Fe(CN)_6$. (b) Optical micrograph of the same surface region where the probe current image was measured. The index planes described on the optical micrograph represent the orientation of each crystal grain evaluated from the etch pit shape. The real deviation from the index plane is described with rotation angles about [100] and [010] axes in the table.

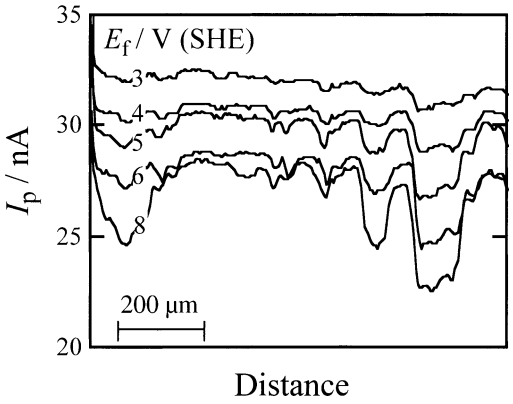


**Fig. 5.** Probe current profiles of the titanium electrode surfaces anodically oxidized at $E_f$=3, 4, 5, 6, and 8 V (SHE), respectively, for 3.6 ks. For measurement, the probe and titanium electrodes were polarized at 1.2 and −0.4 V (SHE), respectively, in deaerated pH 8.4 borate solution containing 0.03 mol dm$^{-3}$ $K_4Fe(CN)_6$.

nium electrode. It was found that oxygen evolution takes place preferentially on the grain with the thinner film as well as reduction of $Fe(CN)_6^{3-}$ during SECM measurement of TG/SC mode in the solution containing $Fe(CN)_6^{4-}$ as shown in **Fig. 6**. This means that electron transfer reaction through the film for reduction of $Fe(CN)_6^{3-}$ or oxygen evolution depends on the thickness and semiconductive properties of the film. **Figure 7**(a) shows the probe current profiles when a polycrystalline titanium electrode is polarized at several potentials of $E_s$ in 0.1 mol dm$^{-3}$ $H_2SO_4$ solution. The marks, A, B, . . . , and F in Fig. 7(a) represent the position of line scan by the probe electrode, whereas numbers, 2, 3, . . . , and 10 represent $E_s$. It is clear that the changes in probe current depend on position of the line scan and anodic potential. Figure 7(b) shows the probe current at each position normalized with that at position B as a function of anodic oxidation potential. The positions are classified into the following 3 types:

(1) oxygen evolution is relatively poor, independent of potential, corresponding to the area where thicker oxide films form (at positions, D and F).
(2) oxygen evolution is relatively active, dependent on potential, corresponding to the area where the thinner oxide films form (at positions of A and E).
(3) oxygen evolution is relatively poor at potentials less than 4.0 V, but active at 4.0 V (SHE) (at position of C).

This means that the structure changes in oxide film from amorphous to anatase at 4.0 V (SHE) contribute to the passage of current through the film.

## 4. *In-situ* Electrochemical Monitoring and Sensing

As described above, the SECM probe electrode is also effective for detecting the reaction products from specimen surface in solutions. Ferrous and ferric ions could be detected during anodic polarization of iron electrode in pH 2.3 sulfate solution.[23] It was found that the active dissolution rate of iron depends on the substrate grain orientation. From the grain oriented to {110}, iron dissolves more actively than the grain oriented to {111} or {100}. Surface atomic density may be reflected to the difference in dissolution rate.

Furthermore, SECM was applied to detect hydrogen and to analyze the mechanism of galvanic corrosion when magnetite was in contact with carbon steel.[24] Hydrogen evolved from magnetite could be detected during cathodic polarization of magnetite electrode. The current efficiency, 50%,

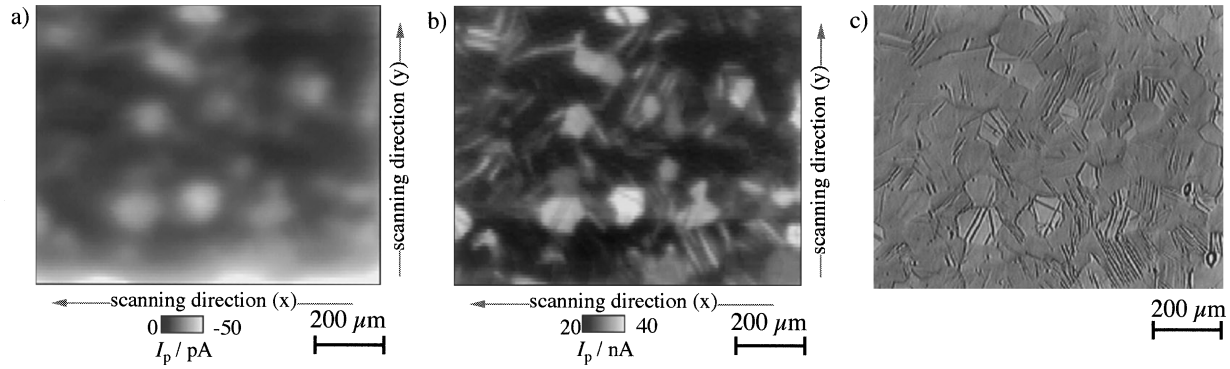


**Fig. 6.** (a) Probe current image of the titanium electrode surface anodically oxidized at 4.0 V (SHE) in 0.1 mol dm$^{-3}$ $H_2SO_4$. The probe electrode was polarized at 0.4 V (SHE). (b) Probe current image measured by conventional SECM in pH 8.4 borate solution containing 0.03 mol dm$^{-3}$ $K_4Fe(CN)_6$ after the experiment of (a). (c) Optical micrograph of the titanium electrode surface where the SECM experiment was performed.

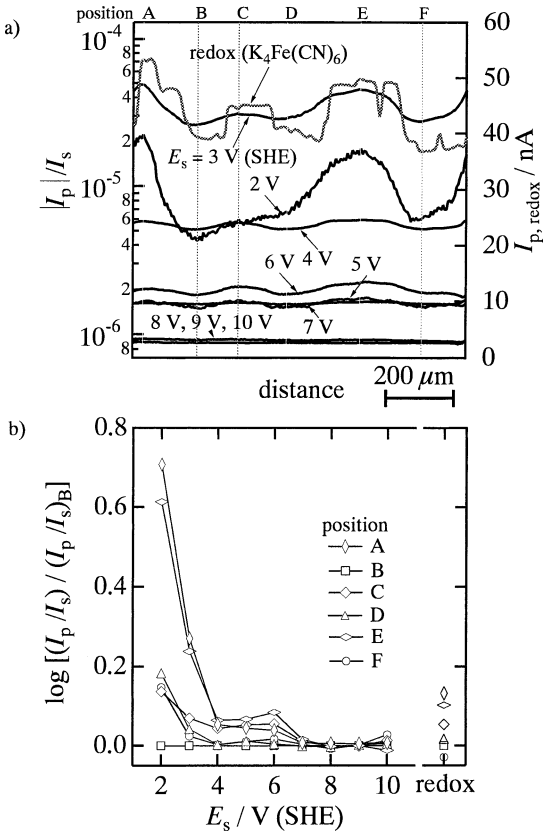


**Fig. 7.** (a) Profiles of normalized oxygen reduction current for the titanium electrode polarized at $E_s$=2.0 to 10 V (SHE) with successive potential steps by 1.0 V in 0.1 mol dm$^{-3}$ $H_2SO_4$ solution and of normalized redox current for the titanium electrode measured in pH 8.4 borate solution containing 0.03 mol dm$^{-3}$ $K_4Fe(CN)_6$ after anodic polarization of the titanium electrode at $E_s$=10 V (SHE) in $H_2SO_4$ solution. The marks, A, B, . . . , F indicate the position of the line scan of probe electrode. (b) The probe current at each position normalized with that at position B as a function of anodic oxidation potential, $E_s$.

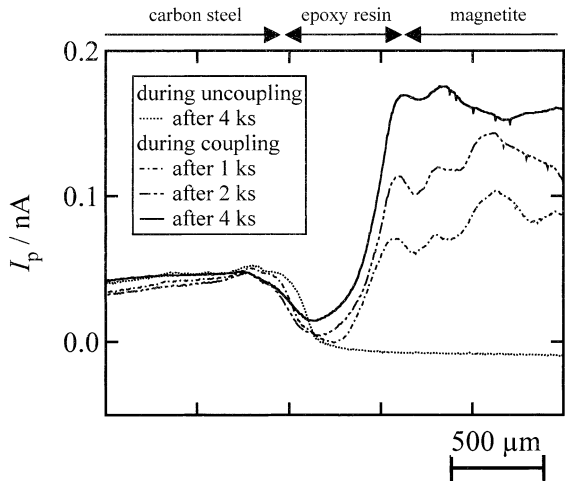


**Fig. 8.** Probe current profiles of carbon steel and single crystal magnetite electrode. The probe electrode was polarized at 0.3 V (SHE) while the carbon steel was coupled or uncoupled with the magnetite in 0.1 mol dm$^{-3}$ $Na_2SO_4$ solution of pH 3.3.

for hydrogen evolution on magnetite electrode was estimated from the comparison with the hydrogen evolution on platinum electrode. **Figure 8** shows the probe current profiles of single crystal magnetite and carbon steel electrodes embedded into epoxy resin in deaerated pH 3.3 sulfate solution. The probe electrode was polarized at 0.3 V (SHE) while the carbon steel electrode was coupled or uncoupled with the magnetite electrode. Since hydrogen is oxidized to protons on the probe electrode at 0.3 V (SHE), the degree of hydrogen generation can be evaluated from the probe current. The probe current at each position corresponds to the concentration of hydrogen generated from the specimen surface. During uncoupling, the probe current is high on the carbon steel electrode as compared with that of the epoxy resin or magnetite electrode. The same current profiles were obtained after 1 ks-uncoupling. On the other hand, during coupling, the probe current profile above the magnetite surface shifts to the anodic direction with time and attains a steady state after 4 ks-coupling. The anodic shift in probe current profiles indicates that hydrogen evolves on the magnetite due to coupling. In contrast, the probe current profile above the carbon steel surface during coupling is not significantly different from that during uncoupling. The significant change in the probe current profile above the magnetite surface during coupling as compared with that above the carbon steel surface indicates that the galvanic corrosion of carbon steel is accelerated by cathodic reaction of the magnetite.

Furthermore it was found that the cathodic polarization

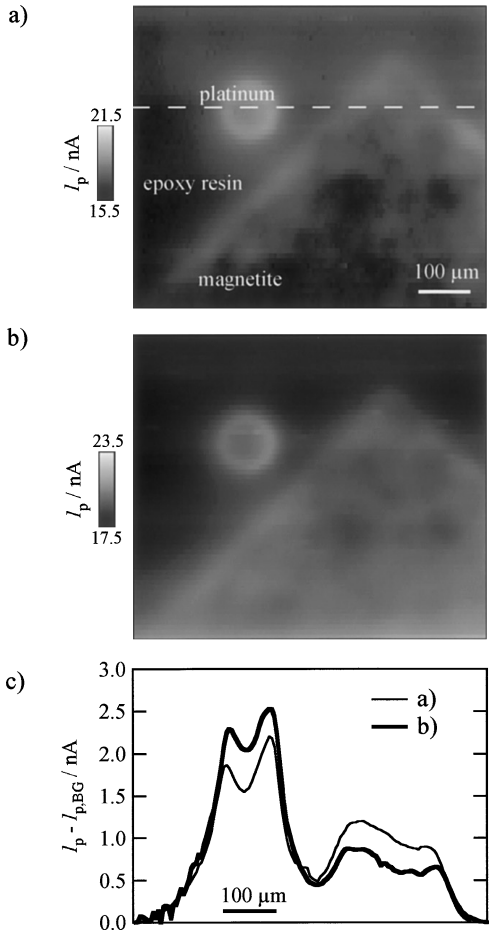


**Fig. 9.** SECM images of feedback mode for the single crystal magnetite and platinum electrodes measured in 0.03 mol dm$^{-3}$ $K_4Fe(CN)_6$ solution, (a) without and (b) after cathodic polarization of magnetite electrode at 1 $\mu$A cm$^{-2}$ for 20 min in pH 3.3 $Na_2SO_4$ solution. The magnetite and platinum electrodes were embedded in epoxy resin. The scanning platinum probe electrode with a diameter of 10 $\mu$m was polarized at 1.2 V (SHE) for the SECM imaging. (c) Probe current profiles subtracted by background current above epoxy resin along the dashed line in a).

of magnetite electrode leads to change in oxidation state of iron to metallic. **Figure 9** shows the SECM images of FB mode for the single crystal magnetite and platinum electrodes measured in pH 8.4, 0.03 mol dm$^{-3}$ $K_4Fe(CN)_6$ solution without and after cathodic polarization of magnetite electrode in pH 3.3 $Na_2SO_4$ solution. The scanning platinum probe electrode polarized at 1.2 V (SHE) oxidizes $Fe(CN)_6^{4-}$ to $Fe(CN)_6^{3-}$. The probe currents above the magnetite and platinum surfaces are relatively high as compared with probe current above the epoxy resin, indicating that reduction of $Fe(CN)_6^{3-}$ takes place easily on both magnetite and platinum surfaces. Moreover, the current above the platinum surface is higher than that above the magnetite surface in Fig. 9(a). This means that $Fe(CN)_6^{3-}$ reduction takes place more difficultly on the magnetite than the platinum. On the other hand, the current above the magnetite surface after cathodic polarization is slightly lower than that above the platinum surface as shown in Fig. 9(b). The alteration causes the increase in surface conductivity of magnetite. The heterogeneity in the probe current images above the magnetite surface may result from fluctuation in chemical composition of the magnetite surface because the electrochemical activity such as reduction of $Fe(CN)_6^{3-}$ is strongly influenced by chemical composition of oxide.

## 5. Liquid-phase Ion Gun to Induce Local Breakdown of Passive Film on Iron

SECM can be employed not only for imaging the distribution of surface electrochemical reactivity but also for inducing a certain surface electrochemical reaction locally on the specimen. It is well known that the local breakdown of passive film on iron is induced in solutions containing chloride ions. When a silver microelectrode covered with silver chloride was employed as a probe electrode and polarized cathodically, chloride ions can be generated from the microelectrode, *i.e.*, operated as an ion gun.[25] The concentration of chloride ions generated from the ion gun in the narrow space between the ion gun and specimen surface with a distance of 75 $\mu$m was estimated about 1 mol dm$^{-3}$ at maximum when an ion gun with a diameter of 180 $\mu$m was polarized at $-0.1$ V (SHE) in pH 6.5 borate solution.[26] The ion gun operating above the passive film on iron electrode induced the local breakdown of the film after several minutes generation of chloride ions as shown in **Fig. 10**.[22] The induction period for the local breakdown depended on film thickness and aging time.[26] Therefore the thinner passive film on grain oriented to {110} had shorter induction period for the breakdown as compared with those on the grains oriented to {111} and {100}.[26] This may give an evidence of liquid-phase ion gun being useful to fabricate the iron electrode surface.

On the other hand, after generation of chloride ions, the ion gun microelectrode can be employed as a detector of ferric ions. From the current transients of the microelectrode and iron electrode, the local breakdown process leading to pit growth due to local enrichment of chloride ions was discussed as follows (see **Fig. 11**).[25]

(1) In domain I, chloride ions are generated from the microelectrode by cathodic polarization and are enriched in the narrow space between the microelectrode and iron electrode due to spatial restriction for diffusion, whereas the iron electrode maintains complete passivity. Therefore, the electric charge, $Q_a$, consumed by the iron electrode is very small in spite of the increase in the electric charge, $Q_c$, consumed by the microelectrode.

(2) In domain II, enriched chloride ions would promote dissolution of passive film as ferric ions into solution. Ferric ions once dissolved from the passive film diffuse to the microelectrode and then are reduced to ferrous ions on the microelectrode. Ferrous ions thus produced on the microelectrode diffuse to the iron electrode and are oxidized again to ferric ions on the iron electrode as far as the passive film is present on iron. This means that a positive feedback mechanism of ferric and ferrous ions via chloride ions is operative between the microelectrode and iron electrode. As passive film thins due to enrichment of chloride ions, the values of $Q_a$ and $Q_c$ increase simultaneously. The ratio of $Q_a/Q_c$ in domain II is nearly unity.

(3) In domain III, a bare surface emerges on the local area of the iron electrode just below the microelectrode due to dissolution of passive film and then active dissolution as

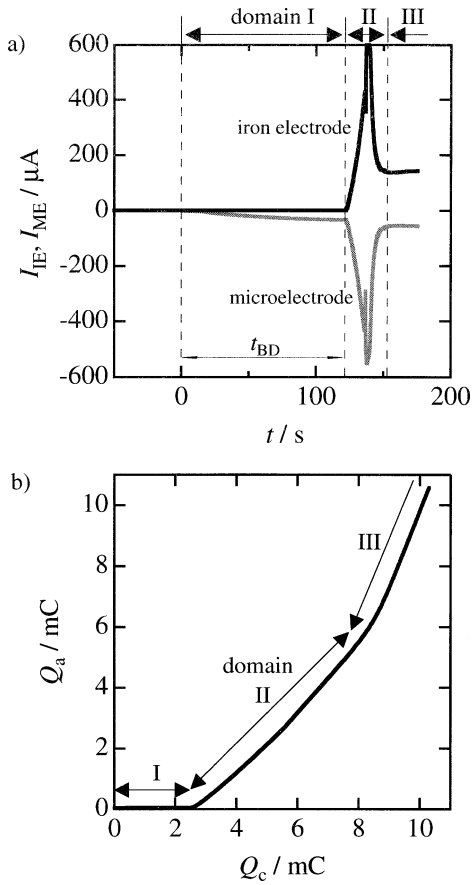


**Fig. 10.** (a) Current transients of microelectrode, $I_{ME}$, and passivated iron electrode, $I_{IE}$, after potential step of the microelectrode from 0.5 V to −0.1 V (SHE), whereas the iron electrode was polarized at 0.7 V (SHE) in deaerated pH 6.5 borate solution. (b) Relation between the electric charges consumed by the microelectrode, $Q_c$, and the iron electrode, $Q_a$.

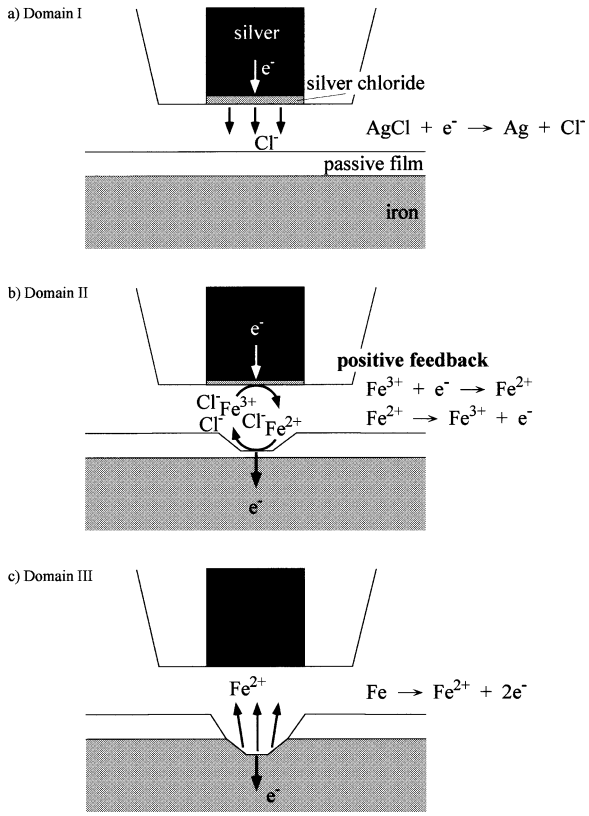


**Fig. 11.** Illustration for the local breakdown processes of the passive film on iron by LPIG. (a) Domain I: a small amount of chloride ions is generated from the microelectrode while the passive film on iron electrode remains stable. (b) Domain II: enriched chloride ions attack the passive film. The film dissolves as ferric ions. Furthermore, the positive feedback takes place between the microelectrode and the iron electrode. (c) Domain III: a bare surface emerges on the local area of the iron electrode surface, from which ferrous ions dissolve and the corrosion pit grows.

ferrous ion proceeds on the local bare surface. Although the dissolved ferrous ions diffuse to the microelectrode, the microelectrode polarized at −0.1 V (SHE) cannot reduce ferrous ions to metallic iron. Moreover, no ferric ions are produced on the iron surface subjected to active dissolution. Therefore, the positive feedback of ferric and ferrous ions between the microelectrode and iron electrode diminishes and finally disappears in domain III, corresponding to negligibly small cathodic current at the microelectrode. The continuous anodic current flow at the iron electrode implies the continuous growth of corrosion pit in depth after complete dissolution of passive film due to chloride ions generated from the microelectrode.

## 6. Conclusions

It is concluded that SECM is useful in evaluating the distribution of electrochemical reactions taking place on the electrode surface such as corrosion reaction, redox reaction on passive film and so on. In the active-dissolution, passive, and oxygen-evolution regions, the heterogeneity of probe current images could detect clearly the distribution of the respective electrochemical reaction over the specimen surface. They depended on the substrate crystallographic orientation. Particularly, on iron in the passive region, the redox reaction of $Fe(CN)_6^{3-}/Fe(CN)_6^{4-}$ proceeded more easily on passive film formed on the grain with high packing density than that on the grain with low packing density, which is mainly due to the difference in film thickness. Moreover, LPIG was developed as a state of art technique to investigate the local breakdown of passive film. Application of LPIG to the passive film formed on iron revealed the details of its local breakdown process.

## REFERENCES

1) R. C. Engstrom, M. Weber, D. J. Wunder, R. Burgess and S. Winquist: *Anal. Chem.*, **58** (1986), 844.
2) A. J. Bard, F.-R. F. Fan, J. Kwak and O. Lev: *Anal. Chem.*, **61** (1989), 132.
3) K. Aoki, M. Morita, T. Horiuchi and O. Niwa: Electrochemical Methods by Using Microelectrodes I, The Institute of Electronics, Information and Communication Engineers, Tokyo, (1998), 4.
4) Y. Saito: *Rev. Polarogr. Jpn.*, **15** (1968) 177.
5) A. J. Bard, F.-R. F. Fan, D. T. Pierce, P. R. Unwin, D. O. Wipf and F. Zhou: *Science*, **254** (1991), 68.
6) A. J. Bard, F.-R. F. Fan and M. V. Mirkin: Electroanalytical Chemistry, Vol. 18, ed. by A. J. Bard, Marcel Dekker, New York, (1994), 243.
7) A. J. Bard and M. V. Mirkin: Scanning Electrochemical Microscopy, Marcel Dekker, New York, (2001).
8) C. Lee and A. J. Bard: *Anal. Chem.*, **62** (1990), 1906.

9) C. Wei and A. J. Bard: *J. Electrochem. Soc.*, **142** (1995), 2523.
10) N. Casillas, P. James and W. H. Smyrl: *J. Electrochem. Soc.*, **141** (1994), L16.
11) N. Casillas, S. Charebois, W. H. Smyrl and H. S. White: *J. Electrochem. Soc.*, **141** (1994), 636.
12) S. B. Basame and H. S. White: *J. Phys. Chem.*, **99** (1995), 16430.
13) S. B. Basame and H. S. White: *J. Phys. Chem.*, **B102** (1998), 9812.
14) K. Fushimi, T. Okawa, K. Azumi and M. Seo: *J. Electrochem. Soc.*, **147** (2000), 524.
15) K. Fushimi, T. Okawa and M. Seo: *Electrochemistry*, **68** (2000), 950.
16) S. B. Basame and H. S. White: *Langmuir*, **15** (1999), 819.
17) S. B. Basame and H. S. White: *Anal. Chem.*, **71** (1999), 3166.
18) K. Fushimi and M. Seo: *Zairyo-to-Kankyo*, **46** (1997), 797.
19) K. Fushimi, K. Azumi and M. Seo: *ISIJ Int.*, **39** (1999), 346.
20) K. Azumi, T. Ohtsuka, and N. Sato: *Denki Kagaku*, **53** (1985), 306.
21) P. James, N. Casillas and W. H. Smyrl: *J. Electrochem. Soc.*, **143** (1989), 3853.
22) N. Casillas, S. Charebois, W. H. Smyrl and H. S. White: *J. Electrochem. Soc.*, **140** (1993), L142.
23) K. Fushimi and M. Seo: *Electrochim. Acta*, **47** (2001), 121.
24) K. Fushimi, T. Yamamuro and M. Seo: *Corros. Sci.*, **44** (2002), 611.
25) K. Fushimi, K. Azumi and M. Seo: *J. Electrochem. Soc.*, **147** (2000), 552.
26) K. Fushimi and M. Seo: *J. Electrochem. Soc.*, **148** (2001), B450.